Petroleum Science 21 (2024) 1683–1698

Contents lists available at ScienceDirect

Petroleum Science

journal homepage: www.keaipublishing.com/en/journals/petroleum-science

Original Paper

Bridging element-free Galerkin and pluri-Gaussian simulation for geological uncertainty estimation in an ensemble smoother data assimilation framework

Bogdan Sebacher [a, *], Remus Hanea [b]

[a] Department of Applied Informatics, Military Technical Academy "Ferdinand I", Bucharest, Bucharest 050141, Romania
[b] Equinor, Sandslivegen 90, 5254 Sandsli, Bergen, Norway

ARTICLE INFO

Article history:
Received 22 January 2023
Received in revised form
14 November 2023
Accepted 26 December 2023
Available online 30 December 2023

Edited by Jie Hao and Meng-Jiao Zhou

Keywords:
Element free Galerkin (EFG)
Adaptive pluri-Gaussian simulation (APS)
Facies distribution estimation
Ensemble smoother with multiple data assimilation (ESMDA)

ABSTRACT

The facies distribution of a reservoir is one of the biggest concerns for geologists, geophysicists, reservoir modelers, and reservoir engineers due to its high importance in the setting of any reliable decision-making/optimization of field development planning. The approach for parameterizing the facies distribution as a random variable comes naturally through using the probability fields. Since the prior probability fields of facies come either from a seismic inversion or from other sources of geologic information, they are not conditioned to the data observed from the cores extracted from the wells. This paper presents a regularized element-free Galerkin (R-EFG) method for conditioning facies probability fields to facies observation. The conditioned probability fields respect all the conditions of the probability theory (i.e. all the values are between 0 and 1, and the sum of all fields is a uniform field of 1). This property achieves by an optimization procedure under equality and inequality constraints with the gradient projection method. The conditioned probability fields are further used as the input in the adaptive pluri-Gaussian simulation (APS) methodology and coupled with the ensemble smoother with multiple data assimilation (ES-MDA) for estimation and uncertainty quantification of the facies distribution. The history-matching of the facies models shows a good estimation and uncertainty quantification of facies distribution, a good data match and prediction capabilities.

1. Introduction

The prior estimation of the facies distribution of a reservoir is very important for the development of any optimal planning of the reservoir. The initial knowledge of geology in terms of facies types, contact between them, sizes, and orientation are gathered, some of them under uncertainty, in the exploration phase of the reservoir. This information comes from core observations, outcrop evaluation, and inversion of the seismic data and is the result of the assessment and interpretation of experts (e.g. geologists, geophysicists, geo-modelers, etc) or the output of complex methodologies involving machine learning procedures (Hall, 2016; Al-Mudhafar, 2017; Lee et al., 2022; Noh et al., 2023). This prior information can be used in two ways. A part of it helps in modeling the geologic architecture of the reservoir. Another part of prior information is mathematically modeled using variables that quantify either uncertainty or certainty of the geology. For instance, geological certainty refers to the type of facies observed at a specific location in the reservoir domain. This is probabilistically modeled using the values 0 or 1 (Sebacher et al., 2013). The geologic uncertainty could be represented by the facies dimensions, facies orientations, prior facies probability fields (cubes), vertical proportion curves, global facies proportions and many others. Any geological simulation model should consider the prior information and conditioning the facies simulation to the available data generating facies instances preserving the geological realism (Linde et al., 2015).

One of the important pieces of information, that the geological simulation needs to be conditioned to, is the probability field of facies. The truncated pluri-Gaussian simulation model (TPS, Galli et al., 1994), the multi-point geostatistical simulation model (MPS, Caers and Zhang, 2004), the sequential indicator simulation

* Corresponding author.
E-mail address: bogdan.sebacher@mta.ro (B. Sebacher).

https://doi.org/10.1016/j.petsci.2023.12.020

model (SISIM, Deutsch and Journel, 1992) have the possibility to generate facies distributions by conditioning the simulation to probability fields (e.g. soft data integration modules).

Sequential indicator simulation was one of the first stochastic methods used to create realistic three-dimensional facies instances. The method is suitable when facies indicators can be modeled with two-point geostatistics which give a high uncertainty related to facies geometry and connectivity (Oyeyemi et al., 2018; Abdolahi et al., 2022). Multi-point geostatistical simulation models are able to create realistic three-dimensional facies realizations conditioning training images to soft data through specialized modules such as the "tau model" (Krishnan et al., 2005). The MPS models are superior to SISIM for simulating realistic channelized fluvial systems, especially for those with strong geometry and continuity (Jha et al., 2014; Al-Mudhafar, 2018; Zhou et al., 2018; Zhang et al., 2022), because the simulation takes into account the multiple point statistics between the domain locations, while SISIM uses two-points geostatistics only. Besides the MPS and SISIM models, the object-based simulation models (OBS), Deutsch and Wang (1996) are able to create realistic complex geological instances with facies having predefined shapes and geometries (Vevle et al., 2018; Zhou et al., 2018) where the simulated fields can be conditioned to facies observations taken at the well locations (Deutsch and Tran, 2002).

Fast model update (FMU, Hanea et al., 2015b) is an integrated and automated workflow for reservoir modeling and characterization, and it is the recommended practice for the modeling and simulation work in Equinor. It connects all steps and disciplines from seismic depth conversion to prediction and reservoir management considering relevant reservoir uncertainty.

FMU delivers an ensemble of geologically consistent and history-matched model realizations that together characterize the reservoir uncertainty. The engine of the assisted history matching process is represented by the ensemble smoother with multiple data assimilation (ES-MDA, Emerick and Reynolds, 2013). Hence, the uncertain parameters of interest should be continuous random variables. The FMU allows updates of the structural model, faults, and rock properties (such as permeability and porosity). The facies modeling is an important step in the modeling workflow. The facies are categorical variables (type A, B, C, etc.), therefore there is a need for a parametrization that will project the discrete variables into continuous ones (probabilities). The most informative data about the facies distribution in a reservoir is the seismic data. Inverted seismic data provides probability cubes for facies distribution in each grid cell of a reservoir model. Hence, it is related to the probability parameterization of the facies. Prior knowledge is the key to a successful assisted history matching process, and it links strongly with the geological concept of the formation present in the reservoir.

The adaptive pluri-Gaussian simulation (APS, Sebacher et al., 2017) is the method that links the input seismic data (cubes), the geological concept (expert knowledge), and the truncated pluri-Gaussian methodology to obtain an ensemble representation of the reservoir which obeys the hard data, follows the geology and can be consistently updated. The APS methodology became the recommended practice in Equinor, for facies modeling and simulations in assets in production since 2017. An example of a comparison between the SISIM method and APS applied for AHM in the Peregrino asset in Brazil is presented in Hanea et al. (2016). Three-dimensional facies simulation with APS was presented in a real field case in Strom et al. (2016), where an ensemble-based history matching technique was employed to consistently condition the dynamic data to facies models.

The probability fields/cubes of facies is one of the main ingredient in the APS methodology, and consequently in the FMU. These fields must be created in such a way that is consistent with the seismic and well-log data. The probability fields of facies inferred from well-log data are, traditionally, calculated with geostatistical algorithms involving kriging interpolation (Deutsch, 2002), but one needs a significant amount of facies data to apply those algorithms.

Another approach is to create, with a geological simulation model, an ensemble of possible realizations of facies fields conditioned on well observations and calculate the probability field of each facies from the ensemble (Sebacher et al., 2013). However, this approach could cause bias due to the geostatistical properties of the random fields used in the generation process of the facies fields (Sebacher et al., 2017) and the seismic data are not taken into account. A different method to build probability fields of facies is by using inversion techniques applied to the seismic data gathered during the exploration phase of the reservoir (Abadpour et al., 2017). Avseth et al. (2001) developed a methodology for generating the probability field of facies involving a Bayesian inversion of the seismic acquisitions, and Ng et al. (2008) present a method for creating the probability fields of the facies combining well log facies information, statistics of the rock physics, and seismic inversion while Massonnat (1999) considered the probability of occurrence of a facies as a function of palaeobathymetry ranges. However, these fields are not conditioned to facies observations.

A numerical method is developed, outside of the geological simulation model, in Marzavan and Sebacher (2021). Here, the finite element method (FEM, Zienkiewicz and Taylor, 1993; Marzavan, 2022a) is used for the construction of the probability field of the facies but considers only the facies observations as input. The method works well under isotropic conditions, but it is not developed for the anisotropic case and also does not take into account prior probability fields of facies or global facies proportions. All the presented methods generate probability fields for facies but without conditioning them both on facies observations at the well locations and seismic information.

This paper presents a novel methodology to condition the prior probability fields of facies to facies observations collected at the well locations. The prior probability fields of facies coming from seismic inversion are not conditioned to the facies data collected from wells. The proposed methodology merges these two pieces of information that are coming from different sources, providing conditioned facies probability fields. The method works even in the absence of seismic information, but using as the prior probability fields, uniform fields calculated based on global facies proportions.

The method is developed in the element-free Galerkin framework (EFG, Nastasescu et al., 2020) with a regularization procedure that consistently combines the prior probability fields and facies observations. This is done in a static regime. The methodology enhances the one presented in Sebacher et al. (2019) in the sense that here, it works for any number of facies types, and the conditioned probability fields respect all the rules of the probability theory (i.e. at each grid cell of any probability field the value is between 0 and 1 and all the probability fields sum up to 1 at each cell). This property is achieved by an optimization procedure under equality and inequality constraints with the gradient projection method.

The helpfulness of having probability fields of facies is further demonstrated by introducing them as input in a history matching process. In the adaptive pluri-Gaussian methodology (APS, Sebacher et al., 2017), they are the main ingredient and are essential for preserving facies observations during the assimilation of data. Consequently, to show their applicability, the conditioned probability fields constructed with the EFG methodology are introduced in an adaptive pluri-Gaussian simulation model and coupled with the ensemble smoother with multiple data assimilation (ES-MDA, Emerick and Reynolds, 2013) for history matching. The goals are the

estimation of facies distribution, its uncertainty quantification, data match, and predictions.

One of the problems of the history matching of facies models is the preservation of the facies observations at the well locations, during the assimilation of data. The estimation of facies distribution in the truncated pluri-Gaussian simulation (TPS) framework coupled with an ensemble Kalman filtering method was first presented in Liu and Oliver (2005), where the prior facies models were conditioned to facies data based on Gaussian field values at the cells with observations. The facies observations were preserved during the history matching with an iterative Kalman filtering process applied to the Gaussian fields. The same conditioning approach was adopted in Agbalaka and Oliver (2008), with a distance-based localization applied to Gaussian fields, and, also in Agbalaka and Oliver (2009) taking into account non-stationary facies proportions based on trends. This approach, however, decreases the variability of the Gaussian fields and, consequently, the variability of the updated ensemble of facies fields. In Astrakova and Oliver (2014), the facies observations at the well locations are preserved by merging an ensemble smoother with an interior-point method with inequality constraints, post-processing procedure that also modifies the Gaussian field values after data assimilation.

In this paper, the facies observations are kept during the history matching process without any extra conditioning, due to the main property of the adaptive pluri-Gaussian simulation method. In the APS model, this problem is automatically solved by the probability fields that are conditioned on facies observations (Sebacher et al., 2017). We history match the facies models generated from the conditioned probability fields having as the observations, the production data, and global facies proportions. The history-matching result shows a good estimation and uncertainty quantification of facies distribution, a good data match, and very well prediction capabilities.

The paper is organized as follows, in the next section is presented the EFG methodology and its customized implementation to work for probability fields of facies. Section 3 presents the facies simulation with the adaptive pluri-Gaussian method (APS) and probability fields of facies constructed with the EFG methodology. Section 4 contains the implementation of the history matching method and the case study results. The paper ends with conclusions.

2. Element-free Galerkin setup

This section presents the element-free Galerkin (EFG) procedure and its customized implementation applied for conditioning the prior probability fields of facies to facies observations taken at the well locations.

2.1. Element free Galerkin (EFG)

The element-free Galerkin is an interpolation technique in which the function approximation at the unsampled locations depends on a weighted influence of the values at sampled locations. Let $D \subseteq R^2$ be a discretized bi-dimensional domain and $f : D \rightarrow R$ a real function, defined on D of which values $v_j = f(u_j)$ are known in some locations $\{u_j, j = \overline{1,N}\}$ (N is the number of sampled locations). Based on these values we perform interpolation and approximate the value of function f at each unsampled point $u \in D$. First, we set a cartesian coordinate system on the bi-dimensional space R^2 (this is done in a customized fashion) and assign, for each location u, two coordinates $u = (x, y)$. The value of function f at the location u is approximated with a polynomial expression of degree $m \geq 1$ in the coordinate (x, y), of type,

$$f(u) \simeq f_m(u) = \sum_{0 \leq i+j \leq m} a_{ij}(u) x^i y^j. \tag{1}$$

The optimal coefficients $a(u) = (a_{ij}(u))_{i,j}$, where $0 \leq i + j \leq m$ are the ones that minimize the quadratic cost function,

$$J(a(u)) = \sum_{i=1}^{N} W(\|u - u_i\|)(f_m(u_i) - v_i)^2. \tag{2}$$

In this cost function, the misfit $(f_m(u_i) - v_i)^2$ is weighted with a distance-based function $W : [0, \infty) \rightarrow [0, 1]$. The weight function W is similar with the variogram function in kriging interpolation, and is decreasing, high differential with $W(0) = 1$, and with the property that exists a positive number r so that $W(h) = 0$ for each $h \geq r$. The r value is called the radius of the weight function support, which in the one dimensional case is the interval $[0, r]$.

$$W(h) = \begin{cases} 1 - 6\frac{h^2}{r^2} + 8\frac{h^3}{r^3} - 3\frac{h^4}{r^4} & \text{if } 0 \leq h \leq r \\ 0 & \text{if } h > r \end{cases} \tag{3}$$

In the literature, there are many weight functions used in the EFG procedure (Marzavan, 2022b), but for this study, the function chosen is the quadratic spline function (Eq. (3)) of which representation is shown in Fig. 1. The variable r gives the radius of the support of the weight function. In Eq. (2), the argument of function W is the distance between the nodes u and u_i.

This distance is either the euclidian distance (for the isotropic case) or a distance that accounts for anisotropy (i.e. $dist(u_i, u) = \|u - u_i\|_B = (u - u_i)^T B (u - u_i)$ where B is a 2×2 positive definite symmetric real matrix). Consequently, the optimal coefficients are calculated as $a^*(u) = \text{argmin} J(a(u))$ and the approximation is $f(u) \simeq \sum_{0 \leq i+j \leq m} a_{ij}^*(u) x^i y^j$.

2.2. Regularized element free Galerkin (R-EFG)

2.2.1. R-EFG methodology

The EFG method is applied to condition the prior probability field of the facies to facies observations and is presented for a bi-dimensional case with three facies types. The extension to a case with more than three facies types is straightforward. This study consider a reservoir model in which the geology has three facies types, denoted channel belts, crevasse splays, and floodplain, of

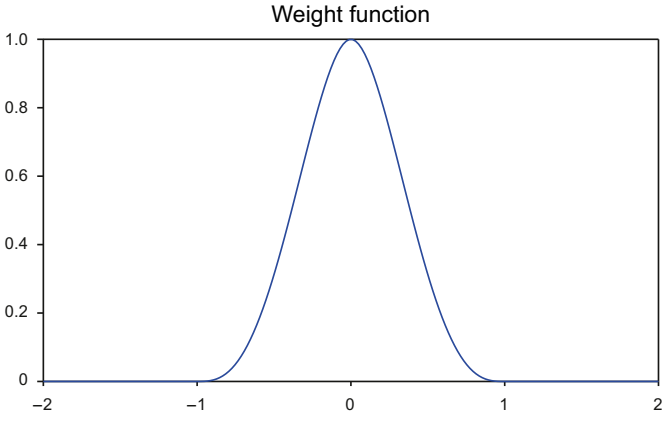

Fig. 1. Weight function in this study.

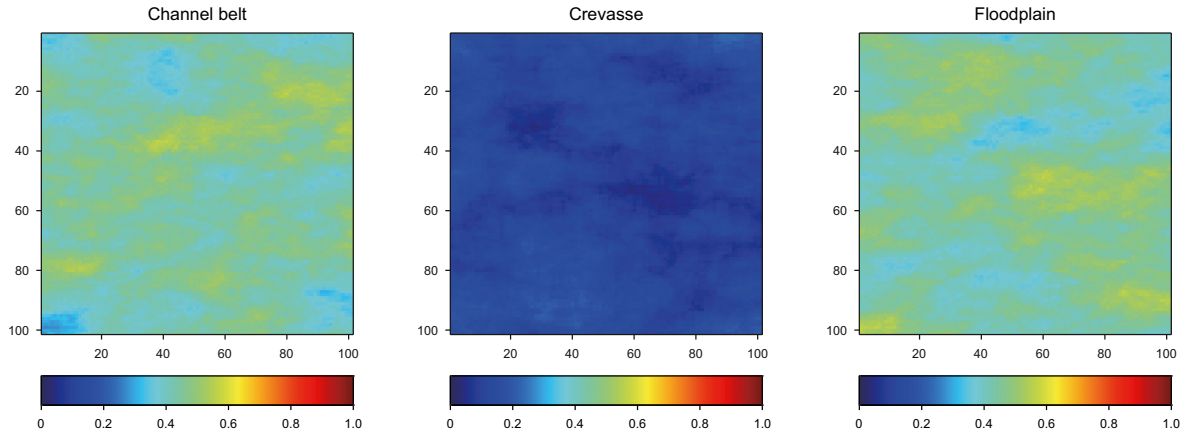

Fig. 2. Prior probability fields of facies types.

which prior probability fields are presented in Fig. 2. The prior geological information about the facies geometry and topology suggests that the channel belts have features with a horizontal orientation and the crevasse splays are small formations situated mainly on the edges of the channel belts.

The floodplain is the geological medium where the other two facies types spatially propagate. We consider an experiment where the reservoir domain is a square with a defined discretization of 100 cells in *Ox* and *Oy* direction. In the EGF methodology, a single piece of information is used for function approximation, the measured values of the function at some locations. In our case, this corresponds to the facies observations at the well locations. To give a numerical meaning to this measurement (a categorical type), we use its probabilistic representation, providing a value of 1 if the facies type is observed and 0 if the facies type is not observed, Fig. 3).

Consequently, each sampled location provides three probabilities, one of 1 and two of 0 (three is the number of facies types that occurs in the reservoir). However, as presented, the EFG method does not incorporate the prior probability fields of the facies. To do this, the cost function from Eq. (2) is modified by adding a Tikhonov regularization term (Eq. (4)).

$$J(a(u)) = \sum_{i=1}^{N} W(\|u-u_i\|)(f_m(u_i)-v_i)^2 + \lambda(f_m(u)-p(u))^2. \quad (4)$$

In Eq. (4), $p(u)$ represents the prior probability of the facies type in cell u, and the regularization term $(f_m(u)-p(u))^2$ accounts for the prior probability field of the facies type. The regularized parameter λ will be used to calibrate the importance of the prior information in the conditioning process.

Let $X = X(u) = \begin{bmatrix} 1 & x & y & x^2 & xy & y^2 & \dots & y^m \end{bmatrix}^{\mathrm{T}}$ be the vector with homogenous forms in the coordinates x and y of the location u, $X_i = X(u_i), a(u) = [a_{ij}]^{\mathrm{T}}_{1\le i+j\le m}$ the vector of coefficients, the weights $w_i = W(\|u-u_i\|)$ and the observations $obs(u_i) = v_i$. Then, $f_m(u) = X^{\mathrm{T}}a(u)$ and the cost function becomes,

$$J(a(u)) = \sum_{i=1}^{N} w_i\left(X_i^{\mathrm{T}}a(u) - obs(u_i)\right)^2 + \lambda\left(X^{\mathrm{T}}a(u) - p(u)\right)^2. \quad (5)$$

The cost function from Eq. (5) is quadratic in parameters, convex and has an unique global minimum that is obtained by setting its gradient to zero $\nabla J(a(u)) = 0$. Then, the optimal values of the parameters $a(u)$ are

$$a^*(u) = \left(\sum_{i=1}^{N} w_i X_i^{\mathrm{T}}X_i + X^{\mathrm{T}}X\right)^{-1}\left(\sum_{i=1}^{N} w_i obs(u_i)X_i + \lambda p(u)X\right). \quad (6)$$

The inverse of the matrix from Eq. (6) is the pseudo-inverse. Finally, the updated value of the probability of facies at location u is,

$$p^{\mathrm{up}}(u) = X^{\mathrm{T}}a^*(u). \quad (7)$$

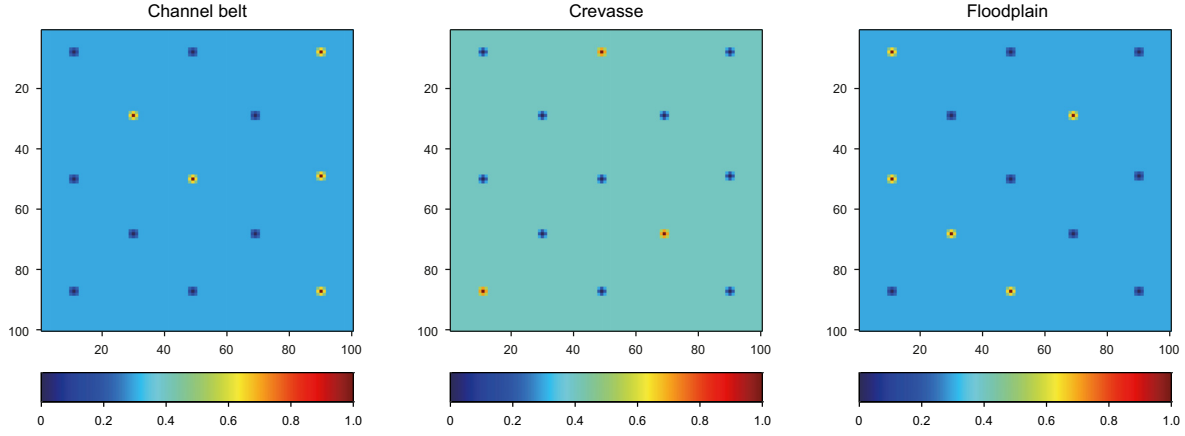

Fig. 3. Facies observations at the well locations.

There are two types of unsampled locations in the reservoir domain, the grid cells that have at least one positive weight and the grid cell for which all the weights are zero. For the second type, the cost function from Eq. (5) becomes $J(a(u)) = \lambda\left(X^{\mathrm{T}}a(u) - p(u)\right)^2$ of which global minimum is 0, obtained for all the parameters that satisfy $X^{\mathrm{T}}a(u) - p(u) = 0$. This means that the updated value of the probability is $X^{\mathrm{T}}a(u) = p(u)$ and is equal to the initial value. Consequently, at the locations where the facies observations have no influence, the prior probabilities do not change. The influence of the facies observations is given by the weight function W by the mean of the radius r of its support. For the implementation, we have used the idea from the finite element theory (Marzavan and Nastasescu, 2022), considering the grid cell as a finite element. Then, for all cells with facies observation, we assign in each node (vertice) of the cell the probability value found in the cell (Fig. 4(a)). This trick multiplies the number of data four times. Consequently, if the discretization of the reservoir domain is 100×100, the EFG method applies for the discretization of 101×101. In this way, the EFG method yields a conditioned probability field for a 101×101 discretization. Then, the conditioned probability fields of each facies type are calculated at the cell level by averaging the values in the nodes of the cells (Fig. 4(b)). In all the experiments, the polynomial function used for approximation is of degree $m = 1$ in coordinates, $f_1(u) = a_1 + a_2x + a_3y$, where $u = (x, y)$. Consequently, $X = [1 \quad x \quad y]^{\mathrm{T}}$ and $a(u) = [a_1 \quad a_2 \quad a_3]^{\mathrm{T}}$.

2.2.2. Results with R-EFG method

Let us apply the EFG method to the reservoir model presented above. The methodology is separately implemented for channel belt, crevasse splay, and floodplain. Knowing that the channel belt has features with a long spatial distribution from east to west but wider from north to south, we choose to apply the weight function setting a distance that accounts for this type of spatial correlation (Eq. (8)):

$$
\begin{aligned}
&W(\|u - u_i\|) = W(r_i)\\
&r_i = \sqrt{\left(\frac{r_i^{(1)}}{\mathrm{long}_r}\right)^2 + \left(\frac{r_i^{(2)}}{\mathrm{short}_r}\right)^2}\\
&r_i^{(1)} = (x - x_i)\cos\alpha + (y - y_i)\sin\alpha\\
&r_i^{(2)} = -(x - x_i)\sin\alpha + (y - y_i)\cos\alpha
\end{aligned}
\tag{8}
$$

In these equations, the angle α is the angle that gives the facies orientation, and long_r and short_r are the radiuses in the principal and secondary directions, respectively. For the floodplain, we choose the same setup as the channel belt, whereas for the crevasse splays, the distance is euclidian (isotropic case). Fig. 5 shows the probability field of channel belt, crevasse, and floodplain obtained conditioning independently of the prior probability fields to facies observations. The parameters used are as follows, for channel belt and floodplain $\mathrm{long}_r = 21$ cells, $\mathrm{short}_r = 7$ cells, $\alpha = 90^\circ$ and for crevasse $\mathrm{long}_r = \mathrm{short}_r = 5$ cells, $\alpha = 0^\circ$.

From the figure, it can be seen that in each cell the values are between 0 and 1, but in some cells, the sum of all probability values is not 1 (picture from the right side of Fig. 5). Consequently, the fundamental condition of the probability theory does not fulfil.

2.3. Regularized element free Galerkin with gradient projection method

To solve this issue, we create a new cost function that incorporates the information from all the probability fields but under constraints. The new constrained optimization problem is defined as follows:

$$
\begin{aligned}
\min J\left(a^1(u), a^2(u), a^3(u)\right) &= \sum_{i=1}^{N} w_i^1\left(X_i^{\mathrm{T}}a^1(u) - obs^1(u_i)\right)^2\\
&+\lambda_1\left(X^{\mathrm{T}}a^1(u) - p^1(u)\right)^2 + \sum_{i=1}^{N} w_i^2\left(X_i^{\mathrm{T}}a^2(u) - obs^2(u_i)\right)^2\\
&+\lambda_2\left(X^{\mathrm{T}}a^2(u) - p^2(u)\right)^2 + \sum_{i=1}^{N} w_i^3\left(X_i^{\mathrm{T}}a^3(u) - obs^3(u_i)\right)^2\\
&+\lambda_3\left(X^{\mathrm{T}}a^3(u) - p^3(u)\right)^2
\end{aligned}
$$

$$
\text{subject to} \quad
\begin{cases}
X_u^{\mathrm{T}}a^1(u) + X_u^{\mathrm{T}}a^2(u) + X_u^{\mathrm{T}}a^3(u) = 1\\
0 \le X_u^{\mathrm{T}}a^1(u) \le 1\\
0 \le X_u^{\mathrm{T}}a^2(u) \le 1\\
0 \le X_u^{\mathrm{T}}a^3(u) \le 1
\end{cases}
\tag{9}
$$

In this equation, variables that are estimated in the minimization problem are $a^i = (a_j^i)_{j=1,2,3}, i = 1, 2, 3$. The parameters $\lambda_1, \lambda_2, \lambda_3$ from Eq. (9) are used for calibrating the influence of the prior probability fields in the conditioning process, so considering that all prior probability fields must have the same impact, the parameter values will be equal $\lambda_1 = \lambda_2 = \lambda_3$. Eq. (9) presents a minimization problem under equality-inequality constraints, but it can be transformed into a minimization problem under inequality constraints only by substituting one of the variables as a function of all the others.

From the equality constrain $X_u^{\mathrm{T}}a^1(u) + X_u^{\mathrm{T}}a^2(u) + X_u^{\mathrm{T}}a^3(u) = 1$ we have $a_1^1(u) = 1 - a_2^1(u)x - a_3^1(u)y - X_u^{\mathrm{T}}a^2(u) - X_u^{\mathrm{T}}a^3(u)$ and a new cost function is defined as follows:

$$
\begin{aligned}
J_1\left(a_2^1, a_3^1, a_1^2, a_2^2, a_3^2, a_1^3, a_2^3, a_3^3\right) = &J\Big(1 - a_2^1x - a_3^1y - X^{\mathrm{T}}a^2\\
&- X^{\mathrm{T}}a^3, a_2^1, a_3^1, a_1^2, a_2^2, a_3^2, a_1^3, a_2^3, a_3^3\Big)
\end{aligned}
$$

(in this equation the current location $u = (x, y)$ is no longer specified). The same substitution modifies all the inequality constraints, and a new minimization problem is defined as follows:

$$
\begin{aligned}
&\min \quad J_1\left(a_2^1, a_3^1, a_1^2, a_2^2, a_3^2, a_1^3, a_2^3, a_3^3\right)\\
&\text{subject to}\\
&\begin{cases}
a_1^2 + a_2^2x + a_3^2y + a_1^3 + a_2^3x + a_3^3y \le 1\\
-a_1^2 - a_2^2x - a_3^2y - a_1^3 - a_2^3x - a_3^3y \le 0\\
a_1^2 + a_2^2x + a_3^2y \le 1\\
-a_1^2 - a_2^2x - a_3^2y \le 0\\
a_1^3 + a_2^3x + a_3^3y \le 1\\
-a_1^3 - a_2^3x - a_3^3y \le 0
\end{cases}
\end{aligned}
\tag{10}
$$

The optimization problem from Eq. (10) is solved with the

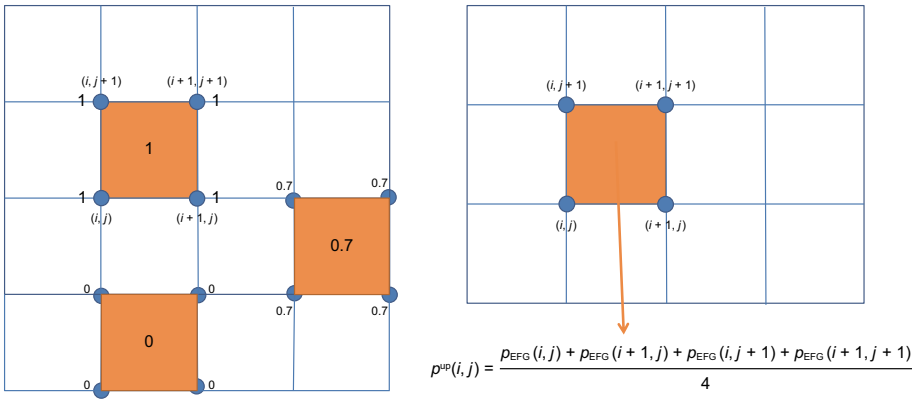

(a) EFG discretization **(b)** EFG update

Fig. 4. Discretization in EFG implementation **(a)** and discretization after EFG update **(b)**.

gradient projection method (GPM, Nocedal and Wright, 2006). The gradient projection method is an iterative method with good results in quadratic optimization under equality and inequality constraints. The method uses the steepest gradient descent but under the condition that, at each iteration, the point remains in the admissible space. To fulfill this condition, the gradient suffers a projection. The problem described in Eq. (10) is rewritten in the form (Eq. (11)) that allows for the implementation of the gradient projection method.

$$\begin{aligned} &\min \quad J_1(a) \\ &\text{subject to } \mathrm{A}\cdot\mathrm{a} \le B \end{aligned} \tag{11}$$

where $a = \left(a_i^j\right)^{\mathrm{T}}$, is the variable vector of dimension 8, A is the 6×8 matrix from the system of constraints (Eq. (10)) and $B = [1 \quad 0 \quad 1 \quad 0 \quad 1 \quad 0]^{\mathrm{T}}$.

A solution consists of a vector $a = \left[a_2^1 \quad a_3^1 \quad a_1^2 \quad a_2^2 \quad a_3^2 \quad a_1^3 \quad a_2^3 \quad a_3^3\right]^{\mathrm{T}}$ for which exist the Lagrange multipliers $\mu = [\ \mu_1 \quad \mu_2 \quad \mu_3 \quad \mu_4 \quad \mu_5 \quad \mu_6\ ]^{\mathrm{T}}$ that fulfill the Karush-Kuhn-Tucker (KKT, Nocedal and Wright, 2006) conditions:

$$\begin{cases} \nabla(J_1(a) + \mu(A\cdot a - B)) = 0 \\ A\cdot a - B \le 0 \\ \mu \ge 0 \\ \text{for each } i\in\overline{1,6} \text{ with } \underbrace{A_i\cdot a - B_i}_{\text{restriction } i} = 0, \text{then } \mu_i > 0 \end{cases} \tag{12}$$

The implementation of the method for our problem consists of two steps, the setup of the starting point and the iterative process (the stopping criterion). For each unsampled location, the initial point could be the one for which all the variables involved in the cost function from Eq. (11) are zero. This corresponds to choosing the probabilities (1,0,0). However, this is not a good choice because the iterative process would be too long. Instead, the primary cost function from Eq. (9) is minimized, and if the solution does not meet the constraints, the variables are projected in the admissible space $(A\cdot a - B \le 0)$. By setting the gradient equal to 0 $(i.e. \nabla J(a^1, a^2, a^3) = 0)$ we obtain the solution,

$$a^{j,*}(u) = \left(\sum_{i=1}^{N} w_i^j X_i^{\mathrm{T}} X_i + X^{\mathrm{T}} X\right)^{-1} \left(\sum_{i=1}^{N} w_i^j obs(u_i) X_i + \lambda p^j(u) X\right),$$

where $j\in\{1,2,3\}$ represents the floodplain, crevasse and channel belt, respectively. In the above equation, the weights are set based on the following rule. If at a location u, is observed a facies type, all the weights $w_i^1 = w_i^2 = w_i^3$ from Eq. (9) are equal and calculated with the weight function having the characteristics given by the facies type observed at the location. This means that, at that location, the observed facies gives the weights for the EFG procedure. The updated probabilities are calculated as $p_j^{\mathrm{up}} = X^{\mathrm{T}} a^{j,*}, j\in\{1,2,3\}$. If these values fulfill the restrictions of Eq. (10) then they are the updated probabilities. If not, we project them in the admissible space (i.e they must belong to [0,1] interval and sum up to 1) and calculate the variables $a_i^j, i,j\in\{1,2,3\}$ that are the initial point in the GPM process. If $p^{\mathrm{up}} = a_1^{\mathrm{up}} + a_2^{\mathrm{up}} x + a_3^{\mathrm{up}} y < 0$, then we define $a_1 = a_1^{\mathrm{up}} - p^{\mathrm{up}}$ which makes the new probability 0. If $p^{\mathrm{up}} = a_1^{\mathrm{up}} +$

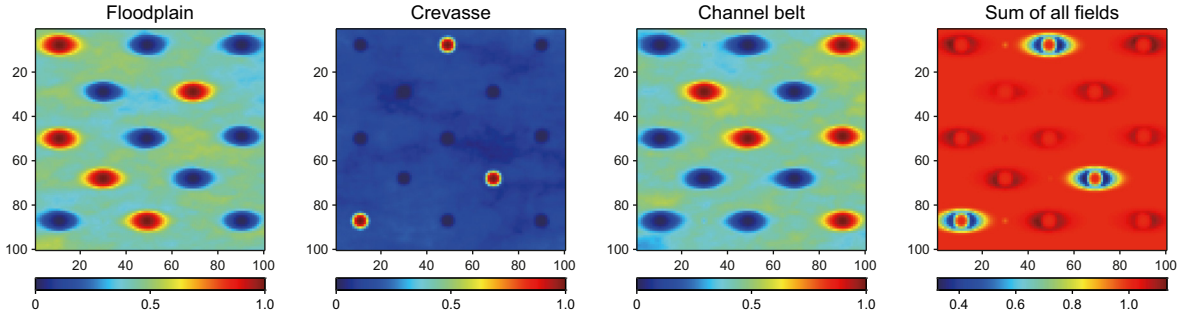

Fig. 5. Conditioned probability fields of facies with EFG implementation.

$a_2^{up}x + a_3^{up}y > 1$, then we define $a_1 = \frac{a_1^{up}}{p^{up}}, a_2 = \frac{a_2^{up}}{p^{up}}, a_3 = \frac{a_3^{up}}{p^{up}}$ which makes the new probability 1. If the sum of all probabilities is not 1, the probabilities are normalized by dividing them by the sum. The above procedure gives the initial guess (starting point) of the iterative GPM process. The i-iteration step of the GPM is

$$a_i = a_{i-1} + \alpha_{i-1} \cdot dir_{i-1} \tag{13}$$

where dir_{i-1} is the direction that can be either $-\nabla J_1(a_{i-1})$, as in steepest gradient descent, or the projection of the $-\nabla J_1(a_{i-1})$ on the space defined only by the tight constraints (the constraints fulfilled with equality) and α_{i-1} is the learning rate. The tight and loose constraints are defined as follows:

$$\begin{cases} \text{Tight constraints} \quad Tc = \{i \in \overline{1,6}, A_i \cdot a - B_i = 0\} \\ \text{Loose constraints} \quad Lc = \{i \in \overline{1,6}, A_i \cdot a - B_i < 0\} \end{cases}. \tag{14}$$

Then,

$$\begin{cases} \text{if} \quad Tc = \varnothing, dir_{i-1} = -\nabla J_1(a_{i-1}) \\ \text{if} \quad Tc \neq \varnothing, dir_{i-1} = -P \cdot \nabla J_1(a_{i-1}), \end{cases} \tag{15}$$

where the projection matrix is $P = I_8 - A_{Tc}^{T} \cdot \left(A_{Tc} \cdot A_{Tc}^{T}\right)^{-1} \cdot A_{Tc}$ and A_{Tc} is the sub-matrix of A constructed with only the coefficients of the tight constraints. The learning rate is calculated in two steps. First, we calculate the learning rate as it comes from the steepest gradient method,

$$\alpha_{i-1}^{(1)} = \underset{t \geq 0}{\operatorname{argmin}} J_1(a_{i-1} + t \cdot dir_{i-1})$$

and second we calculate the learning rate that keeps the point inside of the loose constraints domain,

$$\alpha_{i-1}^{(2)} = \min_{j \in Lc} \left\{ \left| \frac{A_j \cdot a_{i-1} - B_j}{A_{Lc\_j} \cdot dir_{i-1}} \right| - \frac{A_j \cdot a_{i-1} - B_j}{A_{Lc\_j} \cdot dir_{i-1}} > 0 \right\}$$

where A_{Lc} is the submatrix of A, constructed with only loose constraints coefficients, and A_{Lc_j} is the j row of the matrix. Finally,

$$\alpha_{i-1} = \min\left\{\alpha_{i-1}^{(1)}, \alpha_{i-1}^{(2)}\right\}. \tag{16}$$

The Lagrange multipliers, necessary for checking the KKT conditions are calculated based on the following equation, but only for the tight constraints,

$$\mu_{i-1} = \left(A_{Tc} \cdot A_{Tc}^{T}\right)^{-1} \cdot A_{Tc} \cdot dir_{i-1}. \tag{17}$$

The algorithm of the gradient projection method for conditioning the prior probability field of facies to facies observations is presented in the algorithm 1 and applies for the unsampled cell u, of cartesian coordinate $u = (x, y)$ where at least one of the constraints of Eq. (10) do not fulfill.

Algorithm 1: Overview of the algorithm

1. **Calculate** the Initial Guess $a_0 = \left[a_2^1 \quad a_3^1 \quad a_1^2 \quad a_2^2 \quad a_3^2 \quad a_1^3 \quad a_2^3 \quad a_3^3\right]^T$
2. **Calculate** the tight and loose constraints with Eq. (14)
3. **Calculate** the descending direction dir_0 with Eq. (15)
4. **Calculate** the Lagrange multipliers μ_0 with Eq. (17)
5. **Set** the tolerance for the direction norm, denoted *Tol*
6. **Set** $i = 0$
7. **while** $\|dir_0\| > Tol$ and $\min \mu_i < 0$ **do**
8. **Set** $i = i+1$
9. **Calculate** the learning rate α_{i-1} with Eq. (16)
10. **Calculate** the new candidate with Eq. (13)
11. **Calculate** the tight and loose constraints with Eq. (14)
12. **Calculate** the descending direction dir_i with Eq. (15)
13. **Calculate** the Lagrange multipliers μ_i with Eq. (17)
14. **end**

The method was presented for the case of three facies types. However, it can be generalized for any number k of facies types. In this case the constrained optimization problem from Eq. (9) becomes

$$\min J\left(a^1(u), \ldots, a^k(u)\right) = \sum_{j=1}^{k} \left(\sum_{i=1}^{N} w_i^j \left(X_i^T a^j(u) - obs^j(u_i)\right)^2 + \lambda_j \left(X^T a^j(u) - p^j(u)\right)^2 \right)$$

$$\text{subject to} \quad \begin{cases} \sum_{j=1}^{k} X_u^T a^j(u) = 1 \\ 0 \leq X_u^T a^j(u) \leq 1, j \in \{1, \ldots, k\} \end{cases} \tag{18}$$

All the steps necessary to solve the problem from Eq. (18) are similarly with the ones presented in algorithm 1.

2.3.1. Results with the R-EFG implemented with GPM

In the experiments, the tolerance for the euclidian norm of the gradient was set at 10^{-5}.

Fig. 6 presents the conditioned probability field of the channel belt, crevasse, and floodplain (first three figures from left to right) obtained with the optimization procedure based on the gradient projection method and regularized element-free Galerkin. The methodology was implemented on a cell-by-cell basis, but the GPM procedure was necessary for a small number of cells. This happens because, for many locations (with facies observations), the weights are 0, and consequently, the prior probability of that facies does not modify. In addition, for other cells, the constraints were fulfilled by the solution obtained with the unconstrained optimization procedure. The cells for which the GPM iterative process applies are those where more than one location with facies observation has positive weights. However, this phenomenon is controlled by the values of $long_r$ and $short_r$ from the weight function.

From Fig. 6, we can see that all the values of the updated fields are between 0 and 1, and in each cell, the probability fields sum up to 1. The parameters used in the conditioning process are the same as in the initial experiment (i.e. for channel belt and floodplain $long_r = 21$ cells, $short_r = 7$ cells, $\alpha = 90^o$ and for crevasse $long_r = short_r = 5$ cells, $\alpha = 0^o$, while the regularization coefficients $\lambda_1 = \lambda_2 = \lambda_3 = 0.01$. The value of the regularized parameter λ impacts the influence of the prior probability fields in the conditioning process. The higher value of the parameter gives higher importance to the prior probability fields of facies and less impact on the facies observations. This is seen in Fig. 7 where are presented the conditioning results for values of

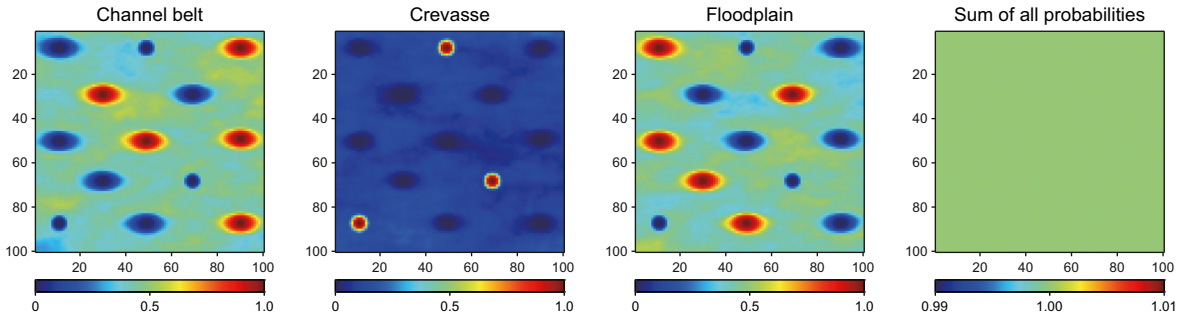

Fig. 6. Conditioned probability fields of facies with GPM and EFG.

$\lambda = 1, 0.1, 0.01, 0.001, 0.0001$ (from top to bottom). Consequently, the setting of this parameter must be done based on the influence we want to give to the facies observations versus prior probability fields. The methodology leaves to the practitioner the freedom to choose their own parameter with which control the influence of the data. If they want to give a higher importance to the prior probability fields they need to increase the value of parameter λ and viceversa. The method applies even for cases where the prior probability fields of facies are not available but are known global facies proportions. Then we consider the prior probability fields of each facies as the uniform fields with the value in each cell equal to the global proportion. This is done in the history matching section.

3. Facies simulation with the adaptive pluri-Gaussian simulation model

The reservoir geology consists of three facies types denoted channel belt, crevasse splay, and floodplain. The prior geological information about the facies geometry and topology suggests that the channel belts have features with a horizontal orientation and the crevasse splays are small formations situated mainly on the edges of the channel belts. The floodplain is the geological medium where the other two facies types spatially propagate. The ingredients of the APS methodology are the Gaussian fields, the simulation map layout, and the prior probability fields of facies. In the pluri-Gaussian simulation framework, we model the geostatistical properties of the Gaussian fields as follows, the first Gaussian field denoted Y_1, anisotropic with a long correlation range of 70 grid cells, short correlation range of 10 grid cells and principal direction horizontal. This Gaussian field models the spatial distribution of the channel belt. The second Gaussian field, denoted by Y_2, is related to the crevasse splays and is chosen isotropic with the correlation range of 10 grid cells. Both Gaussian fields have Gaussian variogram structure and marginally are standard normal.

The construction of the simulation map layout takes into account the topological information of the facies distribution (i.e. the crevasse splays are small formations situated mainly on the edges of the channel belts). Fig. 8 shows the layout of the simulation map of the APS methodology. The simulation (truncation) map consists of a decomposition of the $[0,1] \times [0,1]$ square in three parts, each assigned to a facies type with the area equal to the facies probability.

In this experiment, the prior probability fields of facies are considered uniform fields in each grid cell with the values respectively equal to the expected facies proportions. The expected facies proportions are as follows, 0:43 for the channel belt and floodplain and 0:14 for crevasse splays. Applying the R-EFG method with $\text{long}_r = 21$ cells, $\text{short}_r = 7$ cells, $\alpha = 90^o$ for channel belt and floodplain, and $\text{long}_r = \text{short}_r = 5$ cells, $\alpha = 0^o$ for crevasse and with the regularization coefficients $\lambda_1 = \lambda_2 = \lambda_3 = 0.01$, we obtain the conditioned facies probability fields (Fig. 9).

We denote these probability fields by p_1 for channel belt, p_2 for floodplain, and p_3 for crevasse splays. The facies simulation in the APS methodology consists of taking the following steps as presented in Sebacher et al. (2017),

1. Given the prior probability fields p_1, p_2 and p_3 and information of facies connections, create the layout of the simulation map (Fig. 8).
2. Generate unconditioned samples from the (stationary) Gaussian random fields, Y_1 and Y_2.
3. Transform the Gaussian random fields to uniform random fields, Y_1 and Y_2, using the integral transform. For each j from 1 to 10,000, calculate $\alpha_1^j = \Phi_1(Y_1^j)$ and $\alpha_2^j = \Phi_2(Y_2^j)$ where Φ_1 and Φ_2 are the marginal Gaussian cumulative distribution functions of Y_1 and Y_2.
4. For each j from 1 to 10,000, built the simulation map of the grid cell j from the layout (Fig. 8) and set the facies type in grid cell j, to Facies type k if the point of coordinate $\alpha^j = [\alpha_1^j, \alpha_2^j] \in$ Facies type k area.

The APS methodology ensures the correct conditioning of the simulated facies fields to facies observations (Sebacher et al., 2017). The initial ensemble of facies fields is created by the simulation of $n_e = 120$ pairs of unconditioned Gaussian fields with the previously defined geostatistical properties. For all the experiments, the Gaussian fields were generated with the sequential Gaussian simulation method implemented in SGeMS (the Stanford Geostatistical Software, Remy, 2005). The first three pairs of Gaussian fields and their facies simulations are presented in Fig. 10 where the first row has the first Gaussian field, the second row has the second Gaussian field, and the third row has the facies field simulations with the APS method.

The second main result of the APS method is that if the number of Gaussian field samples goes to infinity, the probability fields of facies calculated from the simulated ensemble of facies fields go to the prior facies probability fields (Sebacher et al., 2017). However, our simulation has only 120 members, but even so, the probability fields of facies calculated from the simulated ensemble, presented in Fig. 11, resemble the prior facies probability fields (Fig. 9).

4. History matching of facies models

The history matching method used for the facies estimation is the ensemble smoother with multiple data assimilation (ES-MDA, Emerick and Reynolds, 2013). This method has been successfully applied for channelized reservoirs simulated with multi-point geostatistical simulation methods (Ma and Jafarpour, 2018; Canchumuni et al., 2019; Sebacher and Toma, 2022) and gave good

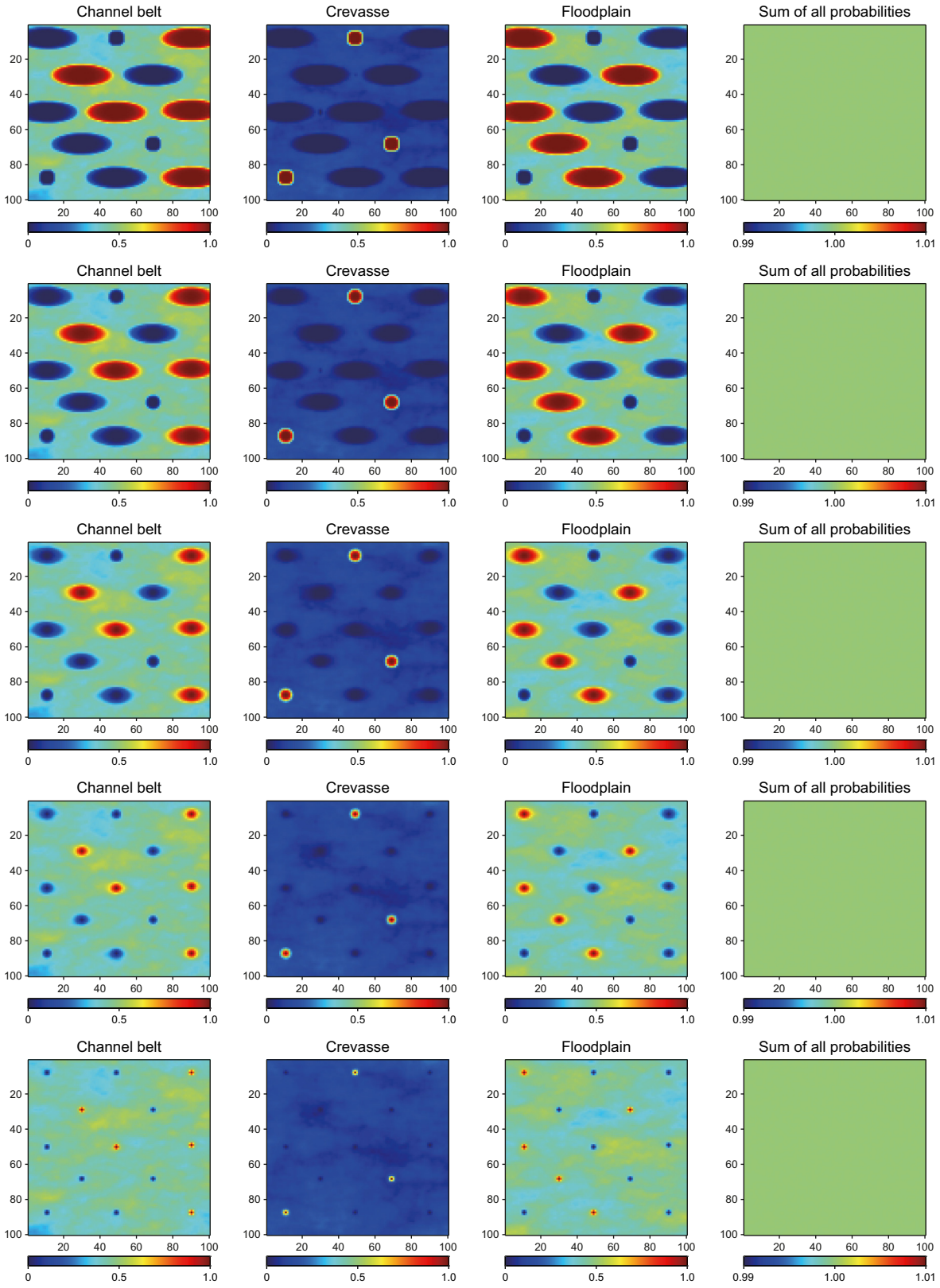

Fig. 7. Conditioned probability fields of facies with GPM and EFG for different values of regularized parameter λ.

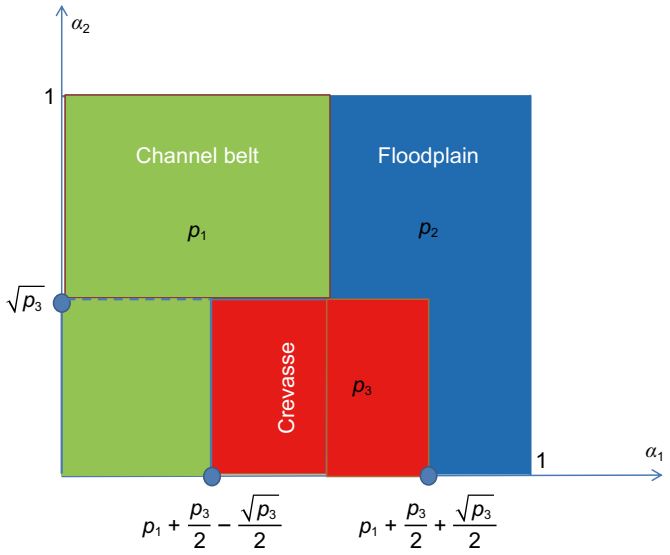

Fig. 8. Simulation map layout in the APS.

results when applied with APS for a real field case (Hanea et al., 2016). The history matching aims the facies estimation and its uncertainty quantification, data match and prediction capabilities of the updated facies models.

4.1. Reservoir model

The reservoir domain is the one presented in Section 2, a square discretized in a number of 10,000 grid cells, each having dimension $30 \times 30 \times 20$ ft. The reservoir geology is of the type previously presented. We design the reservoir model as a water-flooding black oil model, with four injection wells and nine production wells (Fig. 12). The reservoir is filled initially with oil at a constant uniform saturation of 0.8 (the connate water saturation is 0.2) and with a uniform pressure of 3000 psi in every grid cell. The producers work under constant bottom hole pressure (BHP) with a value of 3000 psi, and the injectors operate at 3500 STB/D constrained by a maximum BHP of 100,000 psi. The measurements were gathered through forward simulation of a synthetic model presented as the "reference field". For the construction of the reference model (Fig. 12), a facies model was randomly simulated with APS having as the input the probability fields obtained with the EFG methodology. The simulated facies field was manually adjusted to the shape presented in Fig. 12, where in green is the channel belt, in blue is the floodplain and in red is the crevasse.

The measurement errors of the production data (water rates (WR) and oil rates (OR) at the producers and bottom hole pressures (BHP) at the injectors) are considered Gaussian with 0 mean and standard deviations of 3% from actual measurements. We use these values for generating noisy observations from the reference model. In addition, the Gaussian distribution is used to perturb the observations of production data in the analysis step of the ES-MDA process. Water injection starts from the first day and continues thereafter for 351 days of production. We assimilate data at 60-day intervals resulting in a total of 6 assimilation steps. The permeability values are set at 300 mD for the channel belt, 30 mD for the crevasse, and 3 mD for the floodplain. The porosity is 0.3 for the channel belt, 0.2 for the crevasse, and 0.1 for the floodplain. During the HM process, the permeability and porosity are kept constant, although they could be considered uncertain within each facies and estimated together with facies positions (Hanea et al., 2015a).

4.2. Ensemble smoother with multiple data assimilation (ES-MDA)

In the ensemble smoother with multiple data assimilation (ES-MDA) the observations are iteratively assimilated multiple times, with a number N_a of assimilation cycles (or iterations) a priorly defined. To preserve the mathematical consistency of the method, the error covariance matrix of the observations (C_D) multiplies, at iteration $l \in \overline{1, N_a}$ with a scalar (named inflating factor denoted by α_l) so that $\sum_{l=1}^{N_a} \frac{1}{\alpha_l} = 1$. The last condition ensures that, in the case of a linear (dynamical) model and a Gaussian prior, the updated states are correctly sampling from the Gaussian distribution $p(X|obs)$.

We denote by $m_i^l, i \in \overline{1, n_e}$ the model parameters, at iteration $l \in \overline{1, N_a}$ and by G, the function that projects the parameter values to simulated observations (i.e., $G(m_i^l)$ is the predicted measurements associated to member i). Consequently, the state vector X for the i ensemble member, in iteration l defines as

$$X_i^l = \left[\left(m_i^l\right)^T \quad G\left(m_i^l\right)^T \right]^T, i \in \overline{1, n_e}, \tag{19}$$

where n_e the number of ensemble members and T is the transpose operator. Based on this augmentation, we denote by $H = [0 \quad I]$ the binary matrix that linearly projects X_i^l on the observation space ($HX_l^i = G(m_i^l)$). At each iteration $l \in \overline{1, N_a}$, after the forecast, the

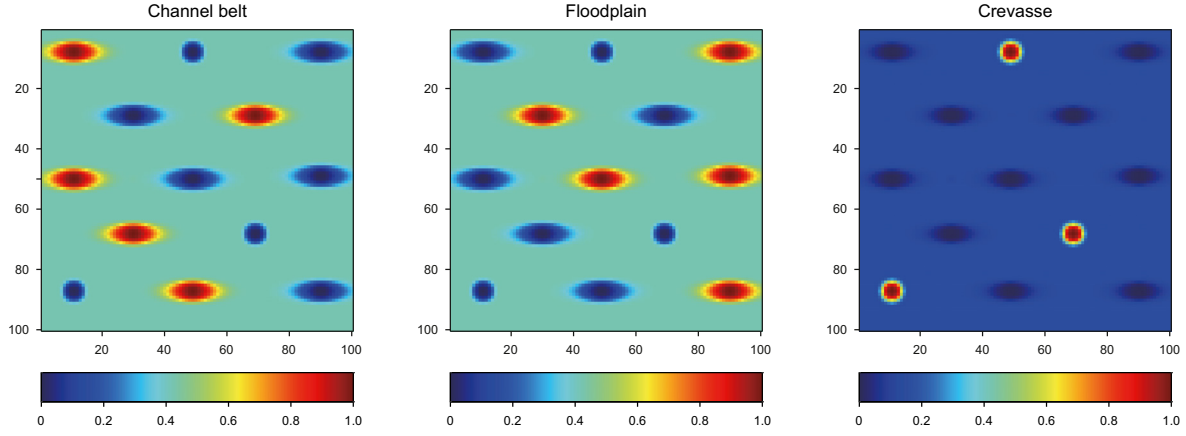

Fig. 9. Conditioned probability fields of facies.

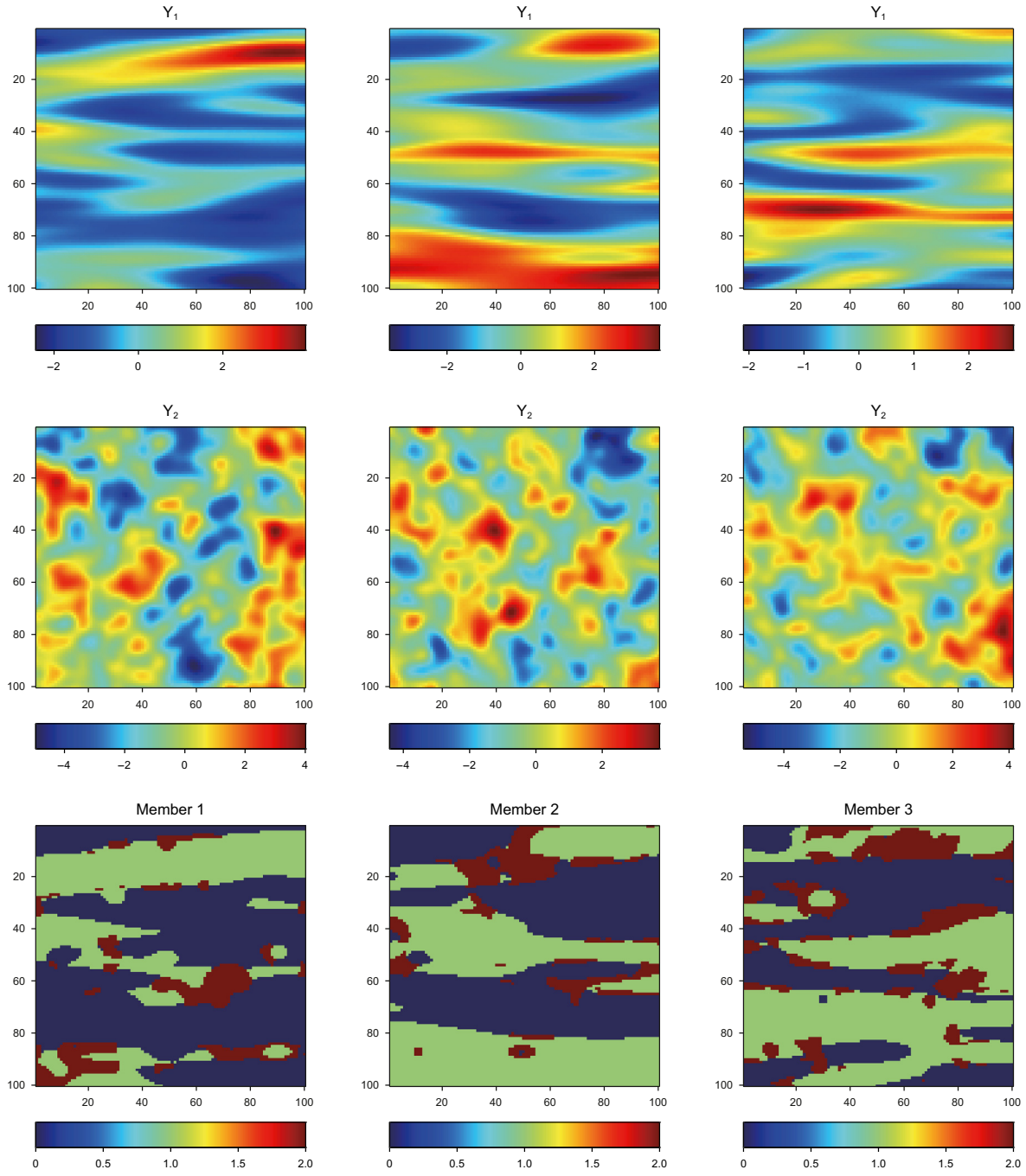

Fig. 10. First three facies simulations with APS.

parameter values remain unchanged (i.e., $m_i^{l,f} = m_i^l$), but, the forecast yields new simulated measurements ($G(m_i^l)$). The parameter values are modified in the updated step when all the observations are assimilated. The Kalman-based equation of the update step is

$$X_i^{l,\mathrm{a}} = X_i^{l,f} + C_{X^{l,f}} H^{\mathrm{T}} \left(H C_{X^{l,f}} H^{\mathrm{T}} + \alpha_l C_D \right)^{-1} \left(d_{\mathrm{obs},i}^l - H X_i^{l,f} \right), \qquad (20)$$

where $X_i^{l,a}$ is the updated (analyzed) state vector, $C_{X^{l,f}}$ is the covariance matrix of the forecasted state vector calculated from the ensemble and $d_{\mathrm{obs},i}^l = d_{\mathrm{obs}} + \varepsilon_i^l$ are the perturbed observations for the ensemble member i at the l-iteration (d_{obs} are the available observations and ε_i^l is a random sampling from a Gaussian distribution with 0 mean and covariance matrix $\alpha_l C_{\mathrm{D}}$). From Eq. (20) of interest are the updated parameters and, retaining the model parameters, it is written as

$$m_i^{l,\mathrm{a}} = m_i^l + C_{m^l, d_{\mathrm{obs}}^l} H^{\mathrm{T}} \left(C_{d_{\mathrm{obs}}^l} + \alpha_l C_{\mathrm{D}} \right)^{-1} \left(d_{\mathrm{obs}} + \varepsilon_i^l - G\left(m_i^l \right) \right). \qquad (21)$$

In Eq. (21), $C_{m^l, d_{\mathrm{obs}}^l}$ is the cross-covariance matrix between the prior model parameters and simulated observations (at iteration l) and

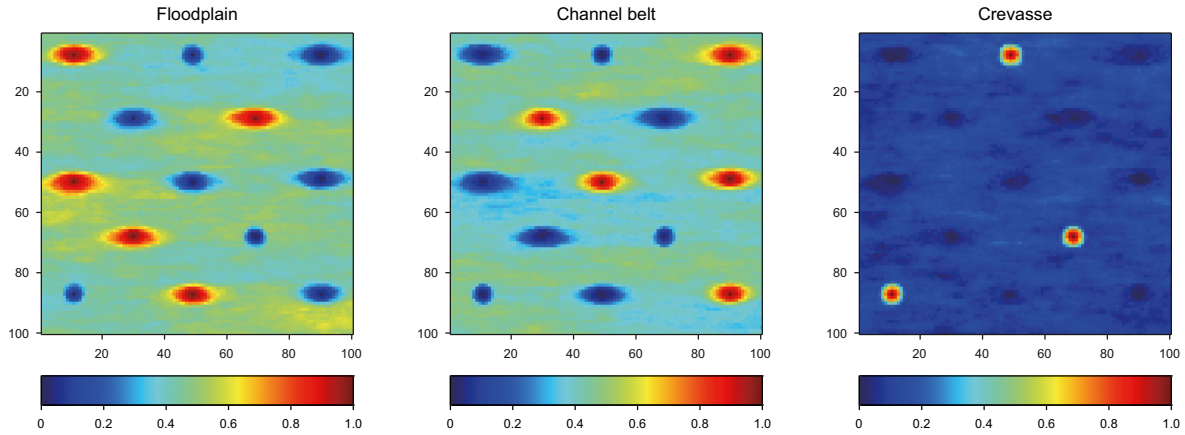

Fig. 11. Facies probability fields calculated from the simulated ensemble.

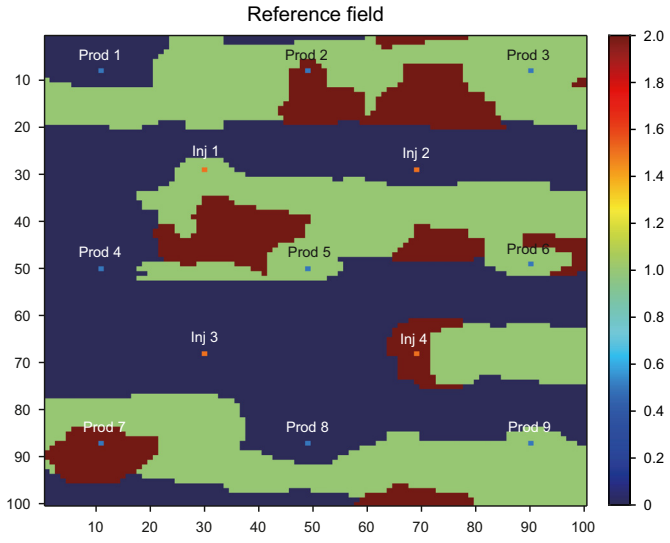

Fig. 12. Reference field.

$C_{d^l_{obs}}$ is the covariance matrix of the simulated observations, at iteration l. Both matrices are calculated from the current ensemble.

4.3. ES-MDA implementation

The ES-MDA method is used with four data assimilations (iterations) with decreasing inflation factors of $(9 : 333 : 7 : 4 : 2)$ with a number of ensembles of $n_e = 120$ members. The state vector for the ensemble member i at the iteration l is defined as

$$X_i^l = \left[Y_1^T \quad Y_1^T \quad BHP^T \quad WR^T \quad OR^T \quad facies\_prop^T \right]_i^{l,T}. \tag{22}$$

The model parameters, in the pluri-Gaussian simulation models, are the sampled Gaussian fields Y_1 and Y_2. The observations used in the history matching process are the bottom hole pressures at the injectors, the water and oil rates at the producers and global facies proportions (Eq. (23)). The facies proportions are considered observations, based on our experience with facies models with more than three types. We have obtained poorer result, in terms of estimation and uncertainty quantification, not considering facies proportion as the observations, fact also proved in Sebacher et al. (2017). The value *facies_prop*, for ensemble member i and facies type k are calculated as,

$$facies\_prop_i^k = \frac{1}{n_g} \sum_{j=1}^{n_g} \mathrm{In}: d_{k,i}(j), \tag{23}$$

where the sum is over all $n_g = 10000$ grid cells and the indicator function for grid cell j is given by,

$$\mathrm{In}: d_{k,i}(j) = \begin{cases} 1 & \text{if cell } j \in \text{facies type } k \text{ for ensemble member } i \\ 0 & \text{if cell } j \notin \text{facies type } k \text{ for ensemble member } i \end{cases}$$

The measured facies proportions are the expected facies proportions, (*floodplain: channelbelt: crevasse*) = (0.43 : 0.43 : 0.14) with an error following a Gaussian distribution with 0 mean and standard deviation of 3% for each facies type. The state vector (Eq. (22)) does not contain the petrophysical properties (permeability, porosity, etc.) of the facies type because these values are kept constant throughout the assimilation period, even though those could be considered uncertain and estimated as in Hanea et al. (2015a). We consider that the uncertainty in the system is due to the poor knowledge of the facies distribution in the reservoir domain.

4.4. History matching results

Fig. 13 shows, at the top, the real position in the reservoir domain of the floodplain, channel belt and crevasse. The pictures are extracted from the reference field (Fig. 12). At the bottom of the same figure are presented the probability fields of the facies calculated from the updated ensemble. By a visual comparison it can be seen a good estimation of the facies position in the reservoir domain, especially for channel belt and floodplain. In addition, from the updated probability fields one can observe that the updated ensemble of facies fields has remained with a good variability. The facies proportion of the reference field are, (*floodplain: channelbelt: crevasse*) = (0.464: 0.405: 0.131) and the average of facies proportions calculated from the updated ensemble is (*floodplain: channelbelt: crevasse*) = (0.4519: 0.4106: 0.1375) close to the reference value. The facies estimation in the reservoir domain can also be evaluated by looking at the individual facies fields in the updated ensemble.

Fig. 14 presents the first three facies fields of the updated ensemble. From the pictures, it can be seen that the main features of the reference field are present in the updated facies fields.

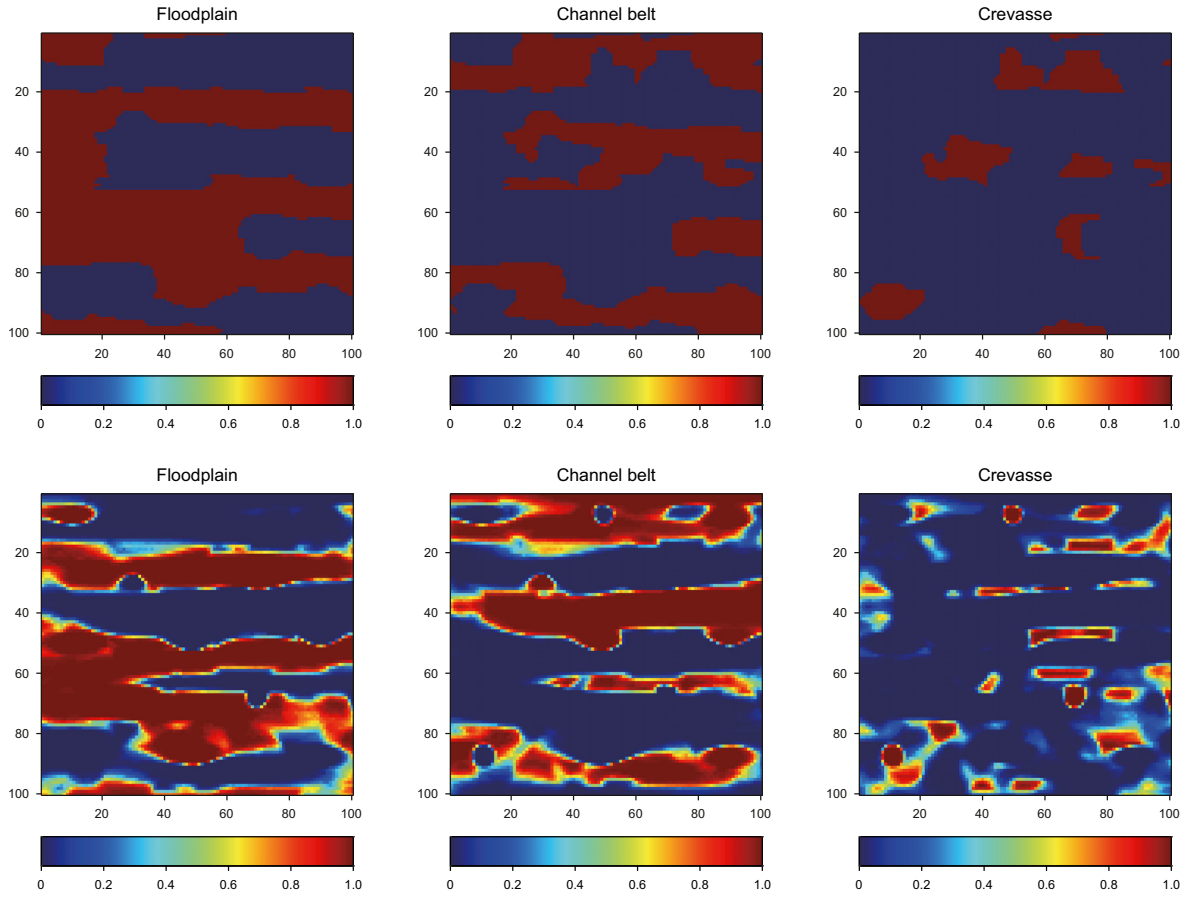

Fig. 13. True position of the facies types (top) and probability fields of facies calculated from the updated ensemble (bottom).

Fig. 15 shows the water rates profiles in the prior ensemble. From the figure, it can be seen that the initial ensemble covers the water rate profiles of the reference field with a high uncertainty.

Fig. 16 shows the water rate profiles in the updated ensemble. From the figure, it can be seen a good reduction in variability, with the updated models covering the water rates profile of the reference field. As an observation, the first two producers do not have water cut during the assimilation period, and this behavior is comprised by the updated facies models.

Fig. 17 shows the water rates prediction for 591 days, the first 351 days represent the data assimilation period, and the next 240 is the prediction period. The blue vertical line delimitates those two periods. From the figure, one can see good prediction profiles, even for the first producer, when all the models do not have water cut yet.

5. Conclusions and discussions

This paper presents a novel methodology to consistently condition the prior probability fields of facies to facies observations.

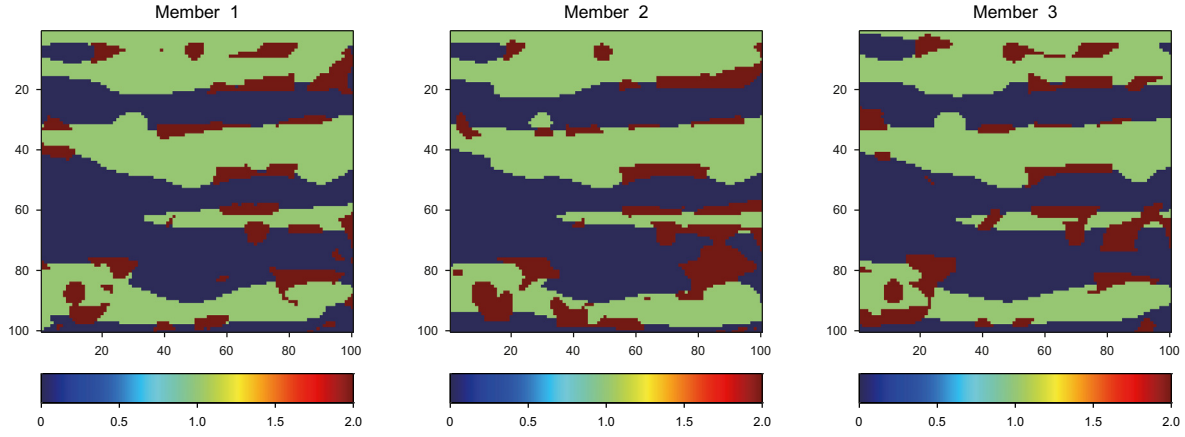

Fig. 14. First three members in updated ensemble.

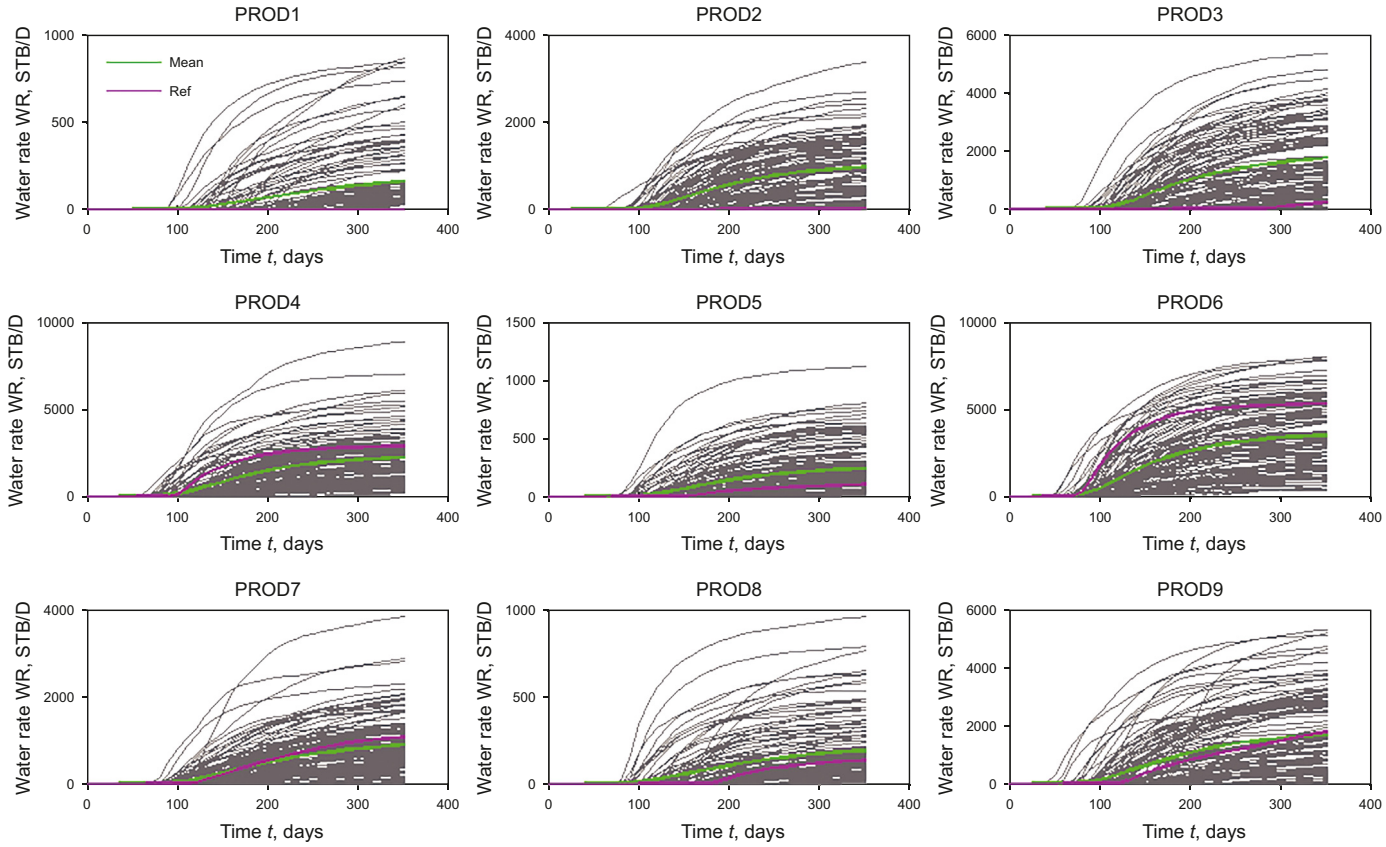

Fig. 15. WR profiles in initial APS ensemble.

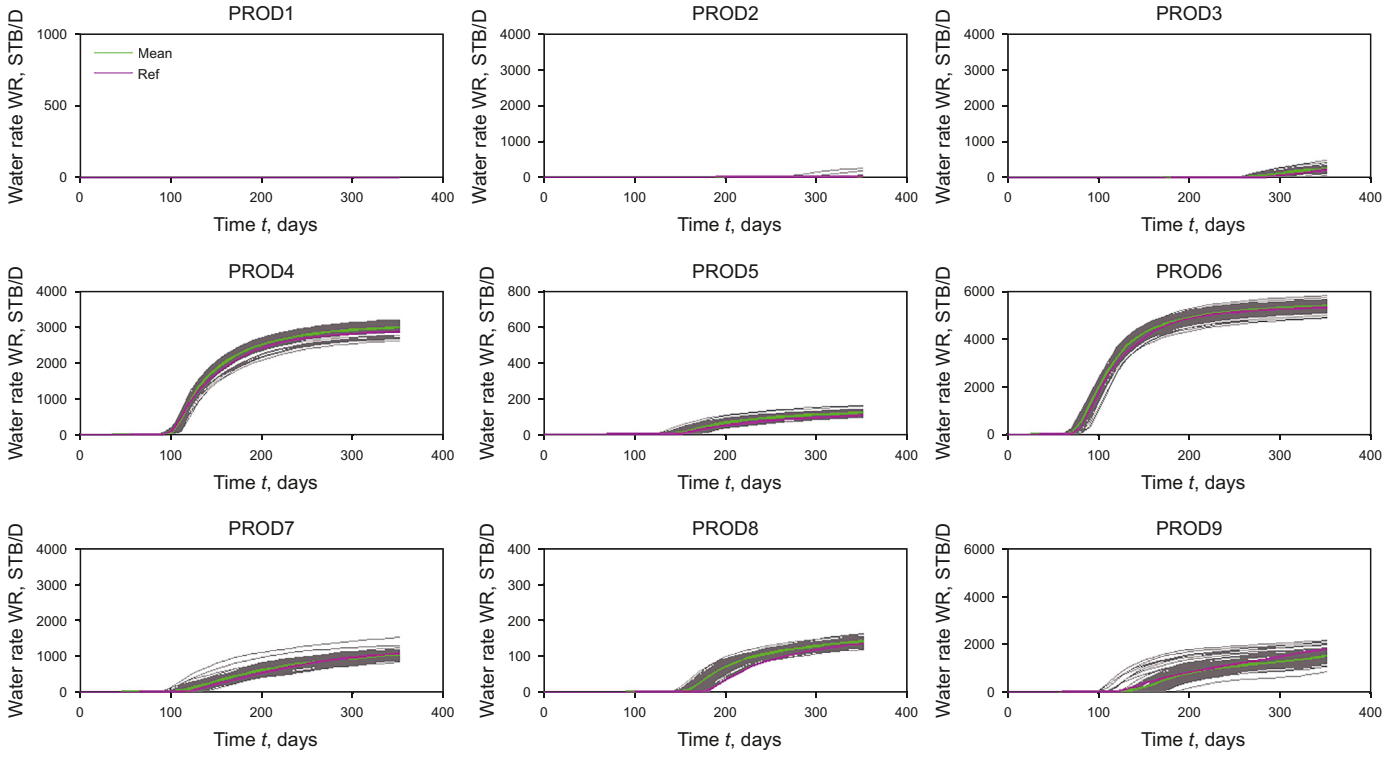

Fig. 16. WR profiles in updated APS ensemble.

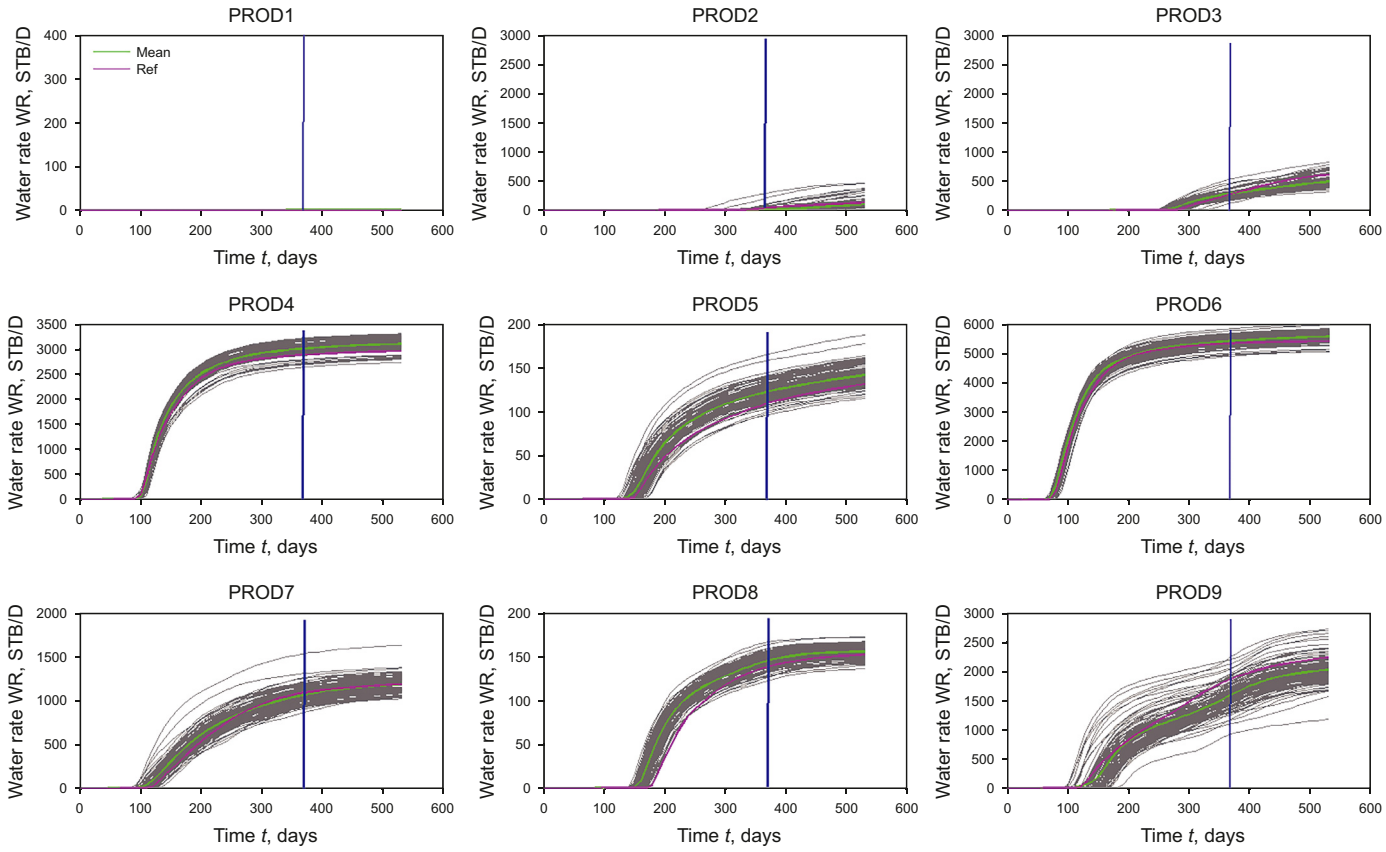

Fig. 17. WR prediction profiles in updated APS ensemble.

These two pieces of information come from different sources. The initial probability fields of facies come after a seismic inversion (soft data) and are usually not conditioned to facies observations. The facies observations are the result after examination of the cores extracted at the well locations (hard data). The method presented in this paper is developed under an element-free Galerkin framework with a Tihonov regularization that accounts for the prior probability fields. To generate probability fields that respect the conditions of the probability theory, is used an optimization technique under equality and inequality constraints involving the gradient projection method. The results are the conditioned probability field for each facies. The methodology leaves the practitioner the freedom to weights the importance of the two sources of information (soft and hard data) based on the parameters of the regularization technique. The conditioned probability fields of facies are input in the adaptive pluri-Gaussian simulation (APS). The conditioning to facies observations is crucial because during the history matching process is not necessary extraconditioning to facies observation. In the paper, the ensemble-smoother with multiple data assimilation (ES-MDA) was chosen as the history-matching algorithm. It was coupled with the APS for the history matching of facies models. The history-matching results show a good estimation and uncertainty quantification of facies distribution, a good data match, and very well prediction capabilities. The method is presented for a bi-dimensional case, representing a layer of a three-dimensional reservoir. The extension to a three-dimensional reservoir must take into account vertical correlations and was not tackled in this study. In addition, the behavior of different weight functions, depending on the specificity of the depositional environments, will be also the subject of a future investigation.

Table 1
Term abbreviations used in this work.

Full Name	Abbreviation
Element-free Galerkin	EFG
Regularized element-free Galerkin	R-EFG
Adaptive pluri-Gaussian simulation	APS
Ensemble smoother with multiple data assimilation	ES-MDA
Truncated pluri-Gaussian simulation	TPS
History matching	HM
Fast model update	FMU
Multi-point geostatistical simulation	MPS
Sequential indicator simulation	SISIM
Object-based simulation	OBS
Finite element method	FEM
Gradient projection method	GPM
Bottom hole pressure	BHP
Water rates	WR
Oil rates	OR

Abbreviations

The abbreviations used in this article are summarized in Table 1.

CRediT authorship contribution statement

Bogdan Sebacher: Writing – review & editing, Writing – original draft, Software, Methodology, Investigation, Formal analysis, Data curation, Conceptualization. **Remus Hanea:** Writing – review & editing, Writing – original draft, Visualization, Validation, Software, Investigation, Formal analysis.

Declaration of competing interest

The author has no relevant financial or non-financial interests to disclose. There is no conflict of interest to publish this work in this journal.

References

Abadpour, A., Adejare, M., Chugunova, T., Deboaisne, R., 2017. Characterization and uncertainty reduction on facies distribution and probability cubes with ensemble Kalman filter history matching. SPE Reservoir Characterisation and Simulation Conference and Exhibition. https://doi.org/10.2118/186074-MS.D031S013R005.

Abdolahi, A., Chehrazi, A., Rahimpour-Bonab, H., Kadkhodaie, A., Seyedali, S., Rao, Y., 2022. Improving the 3D facies model with the seismic-derived log volumes: a case study from the Asmari Formation in the Hendijan Field, southwest Iran. J. Geophys. Eng. 19 (5), 1028–1045. https://doi.org/10.1093/jge/gxac069.

Agbalaka, C.C., Oliver, D.S., 2008. Application of the EnKF and localization to automatic history matching of facies distribution and production data. Math. Geosci. 40 (4), 353–374. https://doi.org/10.1007/s11004-008-9155-7.

Agbalaka, C.C., Oliver, D.S., 2009. Automatic history matching of production and facies data with nonstationary proportions using EnKF. In: SPE Reservoir Simulation Symposium, the Woodlands, Texas. Society of Petroleum Engineers. https://doi.org/10.2118/118916-MS. SPE 118916.

Al-Mudhafar, W.J., 2017. Integrating well log interpretations for lithofacies classification and permeability modeling through advanced machine learning algorithms. J. Pet. Explor. Prod. Technol. 7, 1023–1033. https://doi.org/10.1007/s13202-017-0360-0.

Al-Mudhafar, W.J., 2018. Multiple-point geostatistical lithofacies simulation of fluvial sandrich depositional environment: a case study from Zubair Formation/South Rumaila oil field. SPE Reservoir Eval. Eng. 21 (1), 39–53. https://doi.org/10.2118/187949-PA.

Astrakova, A., Oliver, D.S., 2014. Conditioning truncated pluri-Gaussian models to facies observations in ensemble-Kalman-based data assimilation. Math. Geosci. 47 (3), 345–367. https://doi.org/10.1007/s11004-014-9532-3.

Avseth, P., Mukerji, T., Jørstad, A., Mavko, G., Veggeland, T., 2001. Seismic reservoir mapping from 3-D AVO in a North Sea turbidite system. Geophysics 66 (4), 1157–1176. https://doi.org/10.1190/1.1487063.

Caers, J., Zhang, T., 2004. Multiple-point geostatistics: a quantitative vehicle for integrating geologic analogs into multiple reservoir models. In: Book Chapter, AAPG MEMOIR, Integration of Outcrop and Modern Analogs in Reservoir Modeling. https://doi.org/10.1306/M80924C18.

Canchumuni, S., Emerick, A., Pacheco, M., 2019. History matching geological facies models based on ensemble smoother and deep generative models. J. Petrol. Sci. Eng. 177, 941–958. https://doi.org/10.1016/j.petrol.2019.02.037.

Deutsch, C., Journel, A., 1992. Geostatistical Softwarelibrary and User's Guide. Oxford University Press, New York.

Deutsch, C., Tran, T., 2002. Fluvsim: a program for object-based stochastic modeling of fluvial depositional systems. Comput. Geosci. 28 (4), 525–535. https://doi.org/10.1016/S0098-3004(01)00075-9.

Deutsch, C.V., 2002. Geostatistical Reservoir Modeling. Oxford University Press.

Deutsch, C.V., Wang, L., 1996. Hierarchical object-based stochastic modeling of fluvial reservoirs. Math. Geol. 28 (7), 857–880. https://doi.org/10.1007/BF02066005.

Emerick, A.A., Reynolds, A.C., 2013. Ensemble smoother with multiple data assimilation. Comput. Geosci. 55, 3–15. https://doi.org/10.1016/j.cageo.2012.03.011.

Galli, A., Beucher, H., Le Loc, G., Doligez, B., Heresim Group, 1994. The pros and cons of the truncated Gaussian method. In: Geostatistical Simulations. Springer, pp. 217–233.

Hall, B., 2016. Facies classification using machine learning. Lead. Edge 35 (10), 906–909. https://doi:10.1190/tle35100906.1.

Hanea, R., Ek, T., Sebacher, B., 2015a. Consistent joint updates of facies and petrophysical heterogeneities using an ensemble based assisted history matching. Petrol. Geostat. 2015. https://doi.org/10.3997/2214-4609.201413598.

Hanea, R., Evensen, G., Hustoft, L., Ek, T., Chitu, A., Wilschut, F., 2015b. Reservoir management under geological uncertainty using fast model update. In: 2015 of SPE Reservoir Simulation Conference. SPE-173305-MS.

Hanea, R., Ek, T., Massart, B., Pettan, C., 2016. Quantifying and updating facies uncertainties using ES-MDA - real field case study. In: 78th EAGE Conference and Exhibition. European Association of Geoscientists & Engineers. SPE 118916. https://doi.org/10.3997/2214-4609.201600739.

Jha, S.K., Comunian, A., Mariethoz, G., Kelly, B.F.J., 2014. Parameterization of training images for aquifer 3-D facies modeling integrating geological interpretations and statistical inference. Water Resour. Res. 50 (10), 7731–7749. https://doi.org/10.1002/2013WR014949.

Krishnan, S., Boucher, A., Journel, A.G., 2005. Evaluating information redundancy through the tau model. In: Geostatistics Banff 2004. Springer, pp. 1037–1046.

Lee, A.S., Enters, D., Huang, J., S, J., Liou, S., H, Y., Zolitschka, B., 2022. An automatic sediment facies classification approach using machine learning and feature engineering. Commun. Earth Environ. 3, 294. https://doi.org/10.1038/s43247-022-00631-2.

Linde, N., Renard, P., Mukerji, T., Caers, J., 2015. Geological realism in hydrogeological and geophysical inverse modeling: a review. Adv. Water Resour. 86, 86–101. https://doi.org/10.1016/j.advwatres.2015.09.019.

Liu, N., Oliver, D., 2005. Ensemble Kalman filter for automatic history matching of geologic facies. J. Petrol. Sci. Eng. 47 (3–4), 147–161. https://doi.org/10.1016/j.petrol.2005.03.006.

Ma, W., Jafarpour, B., 2018. Pilot points method for conditioning multiple-point statistical facies simulation on flow data. Adv. Water Resour. 115, 219–233. https://doi.org/10.1016/j.advwatres.2018.01.021.

Marzavan, S., 2022a. EFG method in numerical analysis of foam materials. Mech. Time-Dependent Mater. 26, 409–429. https://doi.org/10.1007/s11043-021-09494-0.

Marzavan, S., 2022b. On the choice of the weight function and its parameters in the element free Galerkin method. Journal of Military Technology 5 (1), 1–8. https://doi.org/10.32754/JMT.2022.1.02.

Marzavan, S., Nastasescu, V., 2022. Displacement calculus of the functionally graded plates by finite element method. Alex. Eng. J. 61 (12), 12075–12090. https://doi.org/10.1016/j.aej.2022.06.004.

Marzavan, S., Sebacher, B., 2021. A new methodology based on finite element method (FEM) for generation of the probability field of rock types from subsurface. Arabian J. Geosci. 14 (10). https://doi.org/10.1007/s12517-021-07114-2.

Massonnat, G.J., 1999. Breaking of a paradigm: geology can provide 3D complex probability fields for stochastic facies modelling. In: SPE Annual Technical Conference and Exhibition, Houston TX, pp. 329–342. https://doi.org/10.2118/56652-MS.

Nastasescu, V., Iliescu, N., Marzavan, S., 2020. Element-free Galerkin method and finite element method. Which is better? J. Eng. Sci. Innov. 5 (5), 287–298. https://doi.org/10.56958/jesi.2020.5.4.287.

Ng, S., Dahle, P., Hauge, R., Kolbjørsen, O., 2008. Estimation of facies probabilities on the Snorre field using geostatistical AVA inversion. In: 2008 SEG Annual Meeting 9-14 November, Las Vegas, Nevada. Society of Exploration Geophysicists. https://doi.org/10.1190/1.3059282.

Nocedal, J., Wright, S.J., 2006. Numerical Optimization. Springer Series in Operations Research and Financial Engineering, second ed.. Springer, New York. https://doi.org/10.1007/978-0-387-40065-5.

Noh, K., Kim, D., Byun, J., 2023. Explainable deep learning for supervised seismic facies classification using intrinsic method. IEEE Trans. Geosci. Rem. Sens. 61, 1–11. https://doi.org/10.1109/TGRS.2023.3236500.

Oyeyemi, K., Olowokere, M., Aizebeokhai, A., 2018. Depositional models using sequential indicator simulation (SISIM) method: a case history in Western Niger delta. Arab. J. Sci. Eng. 43 (10), 3775–3792. https://doi.org/10.1007/s13369-018-3212-4.

Remy, N., 2005. S-gems: the Stanford geostatistical modeling software: a tool for new algorithms development. Geostat. Banff 2004, 865–871. https://doi.org/10.1007/978-1-4020-3610-1_89.

Strom, J., Phade, A., Vinther, M.L., Munck, T.F., 2016. Consistently integrating static and dynamic data in the facies model description using an ensemble based approach. In: Volume Day 1 Mon, November 14, 2016 of IPTC International Petroleum Technology Conference, D011S004R005. https://doi.org/10.2523/IPTC-18868-MS.

Sebacher, B., Toma, S., 2022. Bridging deep convolutional autoencoders and ensemble smoothers for improved estimation of channelized reservoirs. Math. Geosci. 54, 903–939. https://doi.org/10.1007/s11004-022-09997-7.

Sebacher, B., Hanea, R., Heemink, A., 2013. A probabilistic parametrization for geological uncertainty estimation using the ensemble Kalman filter (EnKF). Comput. Geosci. 17 (5), 813–832. https://doi.org/10.1007/s10596-013-9357-z.

Sebacher, B., Hanea, R., Stordal, A., 2017. An adaptive pluri-Gaussian simulation model for geological uncertainty quantification. J. Petrol. Sci. Eng. 158, 494–508. https://doi.org/10.1016/j.petrol.2017.08.038.

Sebacher, B., Hanea, R., Marzavan, S., 2019. Conditioning the probability field of facies to facies observations using a regularized element-free galerkin (EFG) method. In: Petroleum Geostatistics 2019, Florence, Italy, pp. 1–5. https://doi.org/10.3997/2214-4609.201902249.

Vevle, M., Aarnes, I., Ledsaak, K., Hauge, R., Skorstad, A., 2018. Facies modelling of a reallif fluvial system using a modern object-based algorithm. In: 80th EAGE Conference and Exhibition 2018, pp. 1–5. https://doi.org/10.3997/2214-4609.201800792. Volume 2018.

Zhang, N., Li, S., Chang, L., Wang, C., Li, J., Liang, B., 2022. Study on facies modeling of tight sandstone reservoir using multi-point geostatistics method based on 2D training image; case study of longdong area, ordos basin, China. Minerals 12 (10). https://doi.org/10.3390/min12101335.

Zhou, F., Shields, D., Tyson, S., Esterle, J., 2018. Comparison of sequential indicator simulation, object modelling and multiple-point statistics in reproducing channel geometries and continuity in 2d with two different spaced conditional datasets. J. Petrol. Sci. Eng. 166, 718–730. https://doi.org/10.1016/j.petrol.2018.03.043.

Zienkiewicz, O., Taylor, R., 1993. The Finite Element Method, fourth ed. McGraw-Hill, London.